

## Quasielastic electron-deuteron scattering in the weak-binding approximation

J. J. Ethier,<sup>1,2</sup> N. Doshi,<sup>1,3</sup> S. Malace,<sup>1</sup> and W. Melnitchouk<sup>1</sup>

<sup>1</sup>*Jefferson Lab, 12000 Jefferson Avenue, Newport News, Virginia 23606, USA*

<sup>2</sup>*Department of Physics, College of William and Mary, Williamsburg, Virginia 23185, USA*

<sup>3</sup>*Department of Physics, Carnegie Mellon University, Pittsburgh, Pennsylvania 15213, USA*

(Received 17 February 2014; published 10 June 2014)

We perform a global analysis of all available electron-deuteron (*ed*) quasielastic scattering data using  $Q^2$ -dependent smearing functions that describe inclusive inelastic *ed* scattering within the weak-binding approximation. We study the dependence of the cross sections on the deuteron wave function and the off-shell extrapolation of the elastic electron-nucleon cross sections, which show particular sensitivity at  $x \gg 1$ . The excellent overall agreement with data over a large range of  $Q^2$  and  $x$  suggests a limited need for effects beyond the impulse approximation, with the exception of the very high- $x$  and very low- $Q^2$  regions, where short-range meson exchange and final state interaction effects become more relevant.

DOI: [10.1103/PhysRevC.89.065203](https://doi.org/10.1103/PhysRevC.89.065203)

PACS number(s): 13.75.Cs, 13.60.Hb, 21.45.Bc, 13.40.Gp

### I. INTRODUCTION

The deuteron has long been recognized as an ideal laboratory for studying the dynamics of nucleon-nucleon ( $NN$ ) interactions. In particular, when the four-momentum transfer squared,  $Q^2$ , is of the order of the nucleon mass squared,  $M^2$ , or when the fraction of momentum  $x$  carried by the scattered quarks in the deuteron is in the vicinity of  $x \sim 1$ , the role of short-distance effects in the deuteron wave function becomes more prominent. This region makes it possible to explore the structure of the simplest nuclear bound state directly from the underlying theory of the strong interactions, QCD. Together with the constraints on the long-range structure of the deuteron derived from chiral effective theory, the ultimate goal, of course, is to obtain a quantitative description of the deuteron's structure over all distance scales.

From a more practical perspective, experiments involving electron (or other lepton) scattering from the deuteron targets have provided the main source of information about the structure of the neutron. The absence of free neutron targets has meant that properties such as the neutron's elastic form factors or deep-inelastic structure functions are usually extracted from measurements involving deuterons, using empirical information about the corresponding proton observables and knowledge of the  $NN$  interaction in the deuteron. Use of heavier nuclei necessarily increases the size of the bound state effects, exacerbating the uncertainties introduced through our incomplete knowledge of the nuclear wave function and the reaction mechanism.

A robust extraction of neutron information requires a reliable baseline model which accounts for the standard nuclear physics in the deuteron. This is usually embodied in the nuclear impulse approximation, in which the probe scatters incoherently from individual nucleons in the deuteron [1–3]. Corrections to this framework arise in the form of rescattering or final state interactions between the struck nucleon and the spectator recoil [4–8], as well as meson exchange currents [9,10], nucleon off-shell corrections [11–13], and possible non-nucleonic components of the deuteron wave function. The unambiguous identification of these more exotic

effects is only feasible when the baseline calculations within the impulse approximation can be performed with a sufficient degree of precision.

A successful framework which has been used to describe inclusive inelastic electron scattering from nuclei is the weak-binding approximation (WBA), developed by Kulagin *et al.* and applied to both unpolarized [14–17] and polarized [17–19] scattering from the deuteron, as well as  $^3\text{He}$  [20,21] and heavier nuclei [16]. It was also utilized in the extraction of the free neutron structure function  $F_2^n$  from inclusive deuterium and proton data in the nucleon resonance region [22], and the subsequent verification of quark-hadron duality in the neutron [23,24].

Of course, any general approach that aspires to have predictive power must be able to describe a wider set of observables than just a limited class of reactions. Perhaps the most direct window on the nuclear structure of the deuteron is offered by the process of quasielastic (QE) scattering, where the electron scatters elastically from a proton or neutron bound in the deuteron. A large body of data has been accumulated on QE electron-deuteron scattering over the past few decades, covering a large range of  $Q^2$  (between  $Q^2 \approx 0.1$  and 10 GeV<sup>2</sup>) and energies  $E$  (between  $E \approx 0.2$  and 20 GeV), at forward and backward scattering angles [25,26].

In the impulse approximation the QE cross section is proportional to the light-cone momentum distributions of nucleons in the deuteron,  $f^{N/d}$  (also referred to as the “smearing functions”). These are the same distributions that are used to compute the deuteron structure functions in deep-inelastic scattering [1,2,12–14,16], where they are convoluted with the inelastic structure functions of the bound nucleons. The resulting convolutions depend rather sensitively on the precise structure of both the smearing functions and the nucleon structure functions. For QE scattering, the deuteron structure functions are directly given by  $f^{N/d}$ , multiplied by  $Q^2$ -dependent elastic nucleon form factors. This makes QE scattering the ideal testing ground for models of the deuteron structure and the details of the nucleon momentum distributions.

Despite the extensive work that has been carried out on computing the smearing functions for application to deep-inelastic scattering, using realistic deuteron wave functions and including finite- $Q^2$  corrections, surprisingly there has never been a direct test of the WBA formalism with QE scattering data. In this paper we perform such an analysis, confronting the calculated light-cone momentum distributions with the entire set of available QE cross sections. The level of agreement between the data and theory will reveal the limits of validity of the WBA in the impulse approximation, and the degree to which rescattering or more exotic effects need to be incorporated for a complete description of electron-deuteron scattering.

In Sec. II we review the formalism needed to describe electron-deuteron scattering in the QE region and outline the derivation of the unpolarized deuteron  $F_1^d$  and  $F_2^d$  structure functions within the WBA. We examine the possible effects of the modification of nucleon structure functions off the mass shell, and estimate the uncertainty on this modification using two different prescriptions for the electromagnetic current commonly invoked in the literature. The calculated QE cross sections are compared in Sec. III with all available data on inclusive electron-deuteron scattering in the QE region, for  $x \gtrsim 1$ . We compare the predictions using the same smearing functions as those utilized in deep-inelastic scattering, including the kinematical, finite- $Q^2$  corrections to the smearing functions derived in the high- $Q^2$  limit. We further investigate the dependence of the cross sections on the deuteron wave function for several models based on high-precision  $NN$  potentials, as well as on the effects of the nucleon off-shell corrections. A comprehensive comparison with the data such as this allows us to clearly delineate the regions where the impulse approximation is adequate for understanding the essential features of the data, and to identify where additional effects may be needed in future analyses ( $x \gg 1$ ). Finally, in Sec. IV we summarize our findings and discuss their implications for future work.

## II. QUASIELASTIC SCATTERING IN THE IMPULSE APPROXIMATION

In this section we summarize the main results for inclusive electron-deuteron scattering in the impulse approximation. After reviewing the general results for the deuteron structure functions within the framework of the WBA, we describe how the results are applied to the case of elastic scattering from the nucleon bound inside the deuteron. We present results for the case where the bound nucleon structure is assumed to be the same as that for a free nucleon, as well as for the more general case where the off-shell structure of the bound nucleon is explicitly taken into account.

### A. Inclusive cross section and structure functions

The inclusive cross section for the scattering of an incident electron (with four-momentum  $k_\mu$ ) from a deuteron target ( $P_\mu$ ) to a recoil electron ( $k'_\mu$ ) and unobserved hadronic state  $X$ ,

$ed \rightarrow eX$ , is given in the target rest frame by

$$\frac{d^2\sigma}{d\Omega dE'} = \frac{\alpha^2 E'}{Q^4 E} \frac{1}{M_d} L_{\mu\nu} W^{\mu\nu}, \quad (1)$$

where  $\alpha$  is the electromagnetic fine structure constant,  $E$  ( $E'$ ) is the incident (scattered) electron energy, and  $M_d$  is the deuteron mass. The invariant mass squared of the exchanged photon is given by  $Q^2 \equiv -q^2 \approx 4EE' \sin^2(\theta/2)$ , where  $\theta$  is the electron scattering angle in the target rest frame, with  $q_\mu = k_\mu - k'_\mu$  the exchanged photon four-momentum. The leptonic tensor in Eq. (1) is given by

$$L_{\mu\nu} = 2k_\mu k'_\nu + 2k'_\mu k_\nu + q^2 g_{\mu\nu}, \quad (2)$$

while the deuteron hadronic tensor  $W^{\mu\nu}$  is parametrized by the deuteron structure functions  $F_1^d$  and  $F_2^d$ ,

$$W^{\mu\nu}(P, q) = \left( -g^{\mu\nu} + \frac{q^\mu q^\nu}{q^2} \right) F_1^d + \left( P^\mu - \frac{P \cdot q}{q^2} q^\mu \right) \left( P^\nu - \frac{P \cdot q}{q^2} q^\nu \right) \frac{F_2^d}{P \cdot q}. \quad (3)$$

In terms of the deuteron structure functions, which are usually expressed as functions of  $Q^2$  and the Bjorken scaling variable  $x = Q^2/2Mv$ , where  $v = E - E'$  is the energy transfer, the inclusive cross section can then be written as

$$\frac{d^2\sigma}{d\Omega dE'} = \sigma_{\text{Mott}} \left( \frac{2}{M_d} \tan^2 \frac{\theta}{2} F_1^d(x, Q^2) + \frac{1}{v} F_2^d(x, Q^2) \right), \quad (4)$$

where  $\sigma_{\text{Mott}} = (4\alpha^2 E'^2/Q^4) \cos^2(\theta/2)$  is the Mott cross section for scattering from a point particle. Note that at forward scattering angles ( $\theta \rightarrow 0^\circ$ ) the cross section is given entirely by the  $F_2^d$  structure function, while at backward angles ( $\theta \rightarrow 180^\circ$ ) the  $F_1^d$  structure function is dominant.

### B. Weak-binding approximation

To relate the deuteron cross section or structure functions to those of the nucleon requires modeling of the distribution and interaction of the bound nucleons in the deuterium nucleus. Within a covariant framework the deuteron hadronic tensor  $W^{\mu\nu}$  in Eq. (3) can be written as a product of the nucleon-deuteron scattering amplitude  $\widehat{A}$  and the truncated nucleon hadronic tensor  $\widehat{W}_N^{\mu\nu}$  describing the structure of the off-shell nucleon [12],

$$W^{\mu\nu}(P, q) = \int \frac{d^4 p}{(2\pi)^4} \text{Tr}[\widehat{A}(P, p) \widehat{W}_N^{\mu\nu}(p, q)], \quad (5)$$

where  $p$  is the four-momentum of the struck nucleon. Expanding the nuclear amplitude  $\widehat{A}$  to order  $\mathbf{p}^2/M^2$  in the bound nucleon three-momentum and to order  $\varepsilon/M$  in the energy  $\varepsilon \equiv p_0 - M$ , the deuteron tensor simplifies to an integral over the nonrelativistic deuteron spectral function  $\mathcal{P}$  and the nucleon hadronic tensor  $W_N^{\mu\nu}$  [16],

$$W^{\mu\nu}(P, q) = \int \frac{d^4 p}{(2\pi)^4} \frac{M_d}{M + \varepsilon} \mathcal{P}(\varepsilon, \mathbf{p}) W_N^{\mu\nu}(p, q) + O(|\mathbf{p}|^3/M^3). \quad (6)$$

The spectral function is written in terms of the deuteron wave function  $\psi_d$  as

$$\mathcal{P}(\varepsilon, \mathbf{p}) = (4\pi^3) \delta\left(\varepsilon - \varepsilon_d + \frac{\mathbf{p}^2}{2M}\right) |\psi_d(\mathbf{p})|^2, \quad (7)$$

where the deuteron binding energy  $\varepsilon_d = M_d - 2M$  and the wave function is normalized according to  $\int d^3\mathbf{p} |\psi_d(\mathbf{p})|^2 = 4\pi$ .

Evaluating explicitly the hadronic tensor in Eq. (6) with the spectral function in Eq. (7), and equating the coefficients of the tensor in Eq. (3), one can write the deuteron  $F_1^d$  and  $F_2^d$  structure functions in the WBA in terms of the deuteron wave function  $\psi_d(\mathbf{p})$  and the bound nucleon structure functions  $\tilde{F}_1^N$  and  $\tilde{F}_2^N$  [15–17,27],

$$\begin{aligned} xF_1^d(x, Q^2) &= \sum_N \int \frac{d^3\mathbf{p}}{(2\pi)^3} |\psi_d(\mathbf{p})|^2 \left(1 + \frac{\gamma p_z}{M}\right) \\ &\quad \times \left[ C_{11} \frac{x}{y} \tilde{F}_1^N\left(\frac{x}{y}, Q^2, p^2\right) \right. \\ &\quad \left. + C_{12} \tilde{F}_2^N\left(\frac{x}{y}, Q^2, p^2\right) \right], \end{aligned} \quad (8a)$$

$$\begin{aligned} F_2^d(x, Q^2) &= \sum_N \int \frac{d^3\mathbf{p}}{(2\pi)^3} |\psi_d(\mathbf{p})|^2 \left(1 + \frac{\gamma p_z}{M}\right) \\ &\quad \times C_{22} \tilde{F}_2^N\left(\frac{x}{y}, Q^2, p^2\right), \end{aligned} \quad (8b)$$

where  $\gamma^2 = 1 + 4M^2 x^2 / Q^2$  is a kinematical factor, and the sum runs over  $N = p$  and  $n$ . The variable  $y$  is the light-cone momentum fraction of the deuteron carried by the interacting nucleon,

$$y = \frac{M_d p \cdot q}{M P \cdot q} = \frac{p_0 + \gamma p_z}{M}, \quad (9)$$

and the coefficients  $C_{ij}$  are given by

$$C_{11} = 1, \quad (10a)$$

$$C_{12} = (\gamma^2 - 1) \frac{\mathbf{p}_\perp^2}{4y^2 M^2}, \quad (10b)$$

$$C_{22} = \frac{1}{\gamma^2} \left[ 1 + \frac{(\gamma^2 - 1)}{2y^2 M^2} (2p^2 + 3\mathbf{p}_\perp^2) \right]. \quad (10c)$$

Because the struck nucleon is off its mass shell with virtuality  $p^2 = p_0^2 - \mathbf{p}^2 < M^2$ , where the interacting nucleon's energy is  $p_0 = M_d - \sqrt{M^2 + \mathbf{p}^2}$ , the structure functions  $\tilde{F}_1^N$  and  $\tilde{F}_2^N$  in Eqs. (8) can in principle also depend on  $p^2$ , in addition to  $x$  and  $Q^2$ . In practice, since the binding energy is a small ( $\approx 0.1\%$ ) fraction of the deuteron's mass, and the average nucleon momentum in the deuteron is  $|\mathbf{p}| \sim 130$  MeV, the typical nucleon virtuality  $(p^2)^{1/2}$  is only  $\sim 2\%$  less than the free nucleon mass. As a reasonable first approximation, therefore, one can take the bound nucleon structure functions to be the same as their on-shell limits,  $\tilde{F}_{1,2}^N(x, Q^2, p^2) \approx \tilde{F}_{1,2}^N(x, Q^2, M^2) \equiv F_{1,2}^N(x, Q^2)$ . In this case the  $p^2$  (or  $\mathbf{p}_\perp^2$ ) and  $y$  dependence in Eqs. (8) factorizes, and the integration can be reduced to a one-dimensional

convolution in  $y$  [17],

$$\begin{aligned} xF_1^d(x, Q^2) &= \sum_N \int_x^{M_d/M} dy \left[ f_{11}^{N/d}(y, \gamma) \frac{x}{y} F_1^N\left(\frac{x}{y}, Q^2\right) \right. \\ &\quad \left. + f_{12}^{N/d}(y, \gamma) F_2^N\left(\frac{x}{y}, Q^2\right) \right], \end{aligned} \quad (11a)$$

$$F_2^d(x, Q^2) = \sum_N \int_x^{M_d/M} dy \left[ f_{22}^{N/d}(y, \gamma) F_2^N\left(\frac{x}{y}, Q^2\right) \right], \quad (11b)$$

where the nucleon smearing functions in the deuteron  $f_{ij}^{p/d} = f_{ij}^{n/d} \equiv f_{ij}$  (assuming isospin symmetry) are given by [15–17,27]

$$\begin{aligned} f_{ij}(y, \gamma) &= \int \frac{d^3\mathbf{p}}{(2\pi)^3} |\psi_d(\mathbf{p})|^2 \left(1 + \frac{\gamma p_z}{M}\right) \\ &\quad \times C_{ij} \delta\left(y - 1 - \frac{\varepsilon + \gamma p_z}{M}\right). \end{aligned} \quad (12)$$

In the  $\gamma \rightarrow 1$  limit the functions  $f_{ij}$  can be interpreted as light-cone momentum distributions of nucleons in the deuteron, giving the probability of finding a nucleon with a light-cone momentum fraction  $y$  inside the deuteron. For  $\gamma = 1$  the smearing functions are therefore normalized as

$$\int_0^{M_d/M} dy f_{ii}(y, 1) = 1, \quad \int_0^{M_d/M} dy f_{12}(y, 1) = 0. \quad (13)$$

In this limit the convolutions for  $F_1^d$  and  $F_2^d$  are thus diagonal in the structure function type, since  $C_{12} \rightarrow 0$  as  $\gamma \rightarrow 1$ . At finite values of  $Q^2$  the normalizations (13) no longer hold, and the distributions do not have a probabilistic interpretation. However, in practical calculations it is nonetheless vital to keep the full  $Q^2$  dependence of the smearing functions.

In Fig. 1 the smearing function  $f_{22}(y, \gamma)$  relevant for the  $F_2^d$  structure function is illustrated for different values of  $\gamma$  and for different models of the deuteron wave function. In the  $Q^2 \rightarrow \infty$  limit, the function is strongly peaked around  $y = 1$ , with a maximum value of  $\approx 9$ , but becomes broader with increasing  $\gamma$ , with the peak about half as large for  $\gamma = 2$  and 1/4 as large for  $\gamma = 4$  compared with that in the scaling limit. Note that at  $x = 1$  the value of  $\gamma$  is  $\approx 4.3$ , 2.1, and 1.2 at  $Q^2 = 0.2$ , 1, and 10 GeV<sup>2</sup>, respectively, which covers most of the  $Q^2$  range of the available QE data. The behavior of the  $f_{11}(y, \gamma)$  smearing function is qualitatively similar to that in Fig. 1.

At  $y \approx 1$  the smearing function is determined mostly by the long-distance part of the deuteron wave function, which has relatively weak model dependence. The tails of the distributions at  $|y - 1| \gg 0$ , however, exhibit strong deuteron model dependence, with the WJC-1 wave function [28] giving the hardest distribution (largest tails in  $f_{22}$ ), the CD-Bonn [29] the softest distribution (smallest  $f_{22}$ ), and the Paris wave function [30] intermediate between the two. These features are directly reflected in the model dependence of the structure function contributions to the QE cross sections in Sec. III.

Note that whereas some earlier analyses of QE and inelastic electron-deuteron scattering made use of *ad hoc* prescriptions

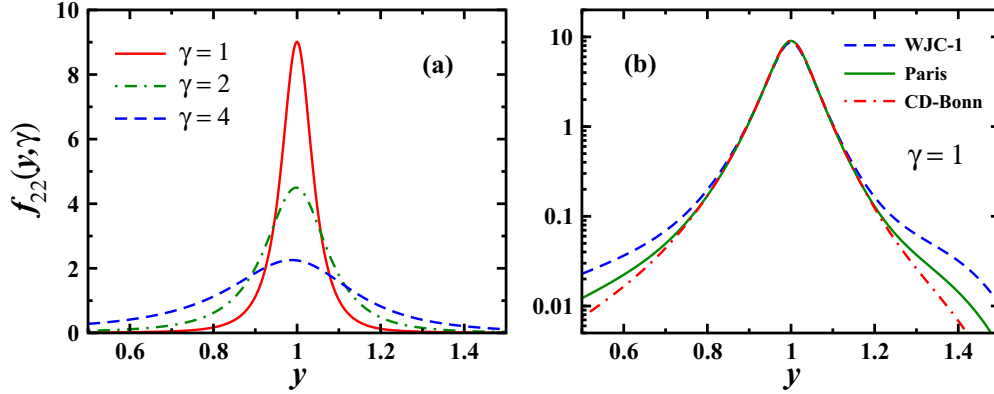


FIG. 1. (Color online) Nucleon smearing function in the deuteron  $f_{22}(y, \gamma)$  as a function of  $y$  for (a) different values of  $\gamma$  ( $\gamma = 1, 2, 4$ ) using the Paris [30] wave function, and (b)  $\gamma = 1$  using the Paris, WJC-1 [28], and CD-Bonn [29] wave functions.

(see Ref. [12] for a discussion), the expressions in Eqs. (8) are systematically expanded in the bound nucleon momentum and are exact to order  $p^2/M^2$  for all values of  $Q^2$ . As discussed above, the only assumption made in Eqs. (11) is that the bound nucleon structure functions appearing in the convolutions are not modified off-shell. The latter assumption constitutes one of the largest sources of uncertainty in the calculation of the deuteron structure functions. In Sec. IID we explore the possible effects of the  $p^2$  dependence of the bound nucleon structure function on the QE cross section. Before doing so, however, we first consider the specific case of elastic scattering from the nucleon.

### C. Quasielastic structure functions

For electron scattering from a free nucleon, the matrix element of the electromagnetic current operator  $J^\mu$  for an elastic final state [ $(p+q)^2 = M^2$ ] is parametrized in terms of the Dirac  $F_{1N}$  and Pauli  $F_{2N}$  form factors [not to be confused with the inclusive structure functions  $F_{1,2}^N(x, Q^2)$ , which are always functions of *two* variables],

$$\begin{aligned} \langle N(p+q) | J^\mu | N(p) \rangle \\ = \bar{u}(p+q) \left[ \gamma^\mu F_{1N}(Q^2) + i\sigma^{\mu\nu} q_\nu \frac{F_{2N}(Q^2)}{2M} \right] u(p), \end{aligned} \quad (14)$$

with the form factors normalized such that  $F_{1p}(0) = 1$ ,  $F_{1n}(0) = 0$ , and  $F_{2N}(0) = \mu_N$ , where  $\mu_N$  is the nucleon anomalous magnetic moment. Using the Gordon identity for on-shell states, one can eliminate the  $\sigma^{\mu\nu}$  term in Eq. (14) to express the matrix element of the electromagnetic current equivalently as

$$\begin{aligned} \langle N(p+q) | J^\mu | N(p) \rangle \\ = \bar{u}(p+q) \left[ \gamma^\mu G_{MN}(Q^2) - (2p^\mu + q^\mu) \frac{F_{2N}(Q^2)}{2M} \right] u(p), \end{aligned} \quad (15)$$

where  $G_{MN}$  here is the Sachs magnetic form factor. The Sachs electric and magnetic form factors are related to the Dirac and

Pauli form factors by

$$F_{1N}(Q^2) = \frac{1}{1+\tau} [G_{EN}(Q^2) + \tau G_{MN}(Q^2)], \quad (16a)$$

$$F_{2N}(Q^2) = \frac{1}{1+\tau} [G_{MN}(Q^2) - G_{EN}(Q^2)]. \quad (16b)$$

As we see in Sec. IID below, the expressions in Eqs. (14) and (15) are equivalent on-shell, but can differ when the initial nucleon is off-shell. In terms of the Sachs electric and magnetic form factors, the elastic contributions to the inclusive structure functions of a free nucleon are given by

$$F_1^{N(\text{el})}(x, Q^2) = \left[ \frac{1}{2} G_{MN}^2(Q^2) \right] Q^2 \delta((p+q)^2 - M^2), \quad (17a)$$

$$\begin{aligned} F_2^{N(\text{el})}(x, Q^2) = \left[ \frac{G_{EN}^2(Q^2) + \tau G_{MN}^2(Q^2)}{1+\tau} \right] \\ \times 2p \cdot q \delta((p+q)^2 - M^2), \end{aligned} \quad (17b)$$

where  $\tau = Q^2/4M^2$ . Using the fact that for an on-shell nucleon ( $p^2 = M^2$ ) one has  $2p \cdot q = 4M^2\tau$ , and the  $\delta$  functions in Eqs. (17) can also be written in terms of the  $x$  variable,  $Q^2 \delta((p+q)^2 - M^2) = 2p \cdot q \delta((p+q)^2 - M^2) = \delta(1-x)$ . Substituting the elastic structure functions in Eqs. (11), the deuteron QE structure functions can then be written as simple products of the nucleon smearing functions  $f_{ij}$  and the elastic electromagnetic form factors,

$$\begin{aligned} x F_1^{d(\text{QE})}(x, Q^2) = \sum_N \left\{ \frac{1}{2} x f_{11}(x, \gamma) G_{MN}^2(Q^2) + x f_{12}(x, \gamma) \right. \\ \left. \times \left[ \frac{G_{EN}^2(Q^2) + \tau G_{MN}^2(Q^2)}{1+\tau} \right] \right\}, \end{aligned} \quad (18a)$$

$$F_2^{d(\text{QE})}(x, Q^2) = \sum_N x f_{22}(x, \gamma) \left[ \frac{G_{EN}^2(Q^2) + \tau G_{MN}^2(Q^2)}{1+\tau} \right]. \quad (18b)$$

The  $Q^2$  dependence of the QE structure functions arises from both the  $Q^2$  dependence of the elastic form factors and the  $\gamma$

dependence of the smearing function. The latter, as we see in Sec. III B, is in fact vital for describing the  $Q^2$  dependence of QE cross section data.

#### D. Nucleon off-shell corrections

For the case where the struck nucleon is bound inside the deuteron and is thus off its mass shell,  $p^2 \neq M^2$ , we can generalize the elastic nucleon scattering contributions

$$\tilde{F}_1^{N(\text{el})}\left(\frac{x}{y}, Q^2, p^2\right) = \left[ \frac{G_{MN}^2}{2} - \frac{(M^2 - p^2)}{2Q^2} \left( \frac{G_{EN}^2 + \tau G_{MN}^2}{1 + \tau} - \frac{(M^2 - p^2)(G_{MN} - G_{EN})^2}{4M^2(1 + \tau)^2} \right) \right] \frac{x}{y} \delta\left(1 - \kappa(p^2)\frac{x}{y}\right), \quad (19a)$$

$$\tilde{F}_2^{N(\text{el})}\left(\frac{x}{y}, Q^2, p^2\right) = \left[ \frac{G_{EN}^2 + \tau G_{MN}^2}{1 + \tau} \right] \delta\left(1 - \kappa(p^2)\frac{x}{y}\right). \quad (19b)$$

This corresponds to what is known in the literature as the ‘‘cc2’’ prescription of De Forest [31].

If one instead uses the form of the electromagnetic current in Eq. (15), the elastic structure functions for the off-shell nucleon are given by the alternative forms

$$\tilde{F}_1^{N(\text{el})}\left(\frac{x}{y}, Q^2, p^2\right) = \left[ \frac{G_{MN}^2}{2} \left(1 - \frac{M^2 - p^2}{Q^2}\right) \right] \frac{x}{y} \delta\left(1 - \kappa(p^2)\frac{x}{y}\right), \quad (20a)$$

$$\tilde{F}_2^{N(\text{el})}\left(\frac{x}{y}, Q^2, p^2\right) = \left[ \frac{G_{EN}^2 + \tau G_{MN}^2}{1 + \tau} - \frac{(M^2 - p^2)(G_{MN} - G_{EN})^2}{4M^2(1 + \tau)^2} \right] \delta\left(1 - \kappa(p^2)\frac{x}{y}\right). \quad (20b)$$

This form corresponds to the ‘‘cc1’’ prescription of Ref. [31].

While the on-shell limits of the two sets of expressions for the structure functions in Eqs. (19) and (20) are equivalent, off-shell these give rise to numerically different results for the QE cross sections. These differences are an indication of the uncertainty in the calculation of the deuteron cross section due to the off-shell extrapolation of the nucleon hadronic tensor, which is discussed in the following section.

### III. NUMERICAL RESULTS

Having derived the results for the contributions of the inclusive deuteron structure functions to the QE cross section within the framework of the WBA, we can now compare the predictions with the available QE electron-deuteron scattering data. In the following we first summarize the data sets used in this analysis before proceeding with the model comparisons.

#### A. Electron-deuteron QE data sets

QE electron-deuteron scattering cross sections have been measured in a number of experiments at several facilities, including SLAC, MIT-Bates, and Jefferson Lab, over a large range of energies and scattering angles. Most of these are summarized in the Quasielastic Electron Nucleus Scattering Archive [25], which includes published data that have been radiatively corrected and are not known to contain any pathologies.

The earliest data set was obtained by Schutz *et al.* [32] from SLAC in the late 1970s, containing forward scattering QE cross sections at  $\theta = 8^\circ$  for incident energies between  $E \approx 6$  and 18 GeV, and extending to very large values of  $x \lesssim 2$ . Backward angle data were obtained by Parker *et al.* [33]

to the structure functions by explicitly taking into account the kinematical  $p^2$  dependence. From the on-shell condition of the final nucleon, one has the constraint  $2p \cdot q = Q^2 + M^2 - p^2 = Q^2/(x/y)$ , where  $y$  is defined in Eq. (9). This enables the  $\delta$  function in Eqs. (17) to be written as  $\delta((p+q)^2 - M^2) = [(x/y)/Q^2] \delta(1 - \kappa(p^2)x/y)$ , where  $\kappa(p^2) = 1 + (M^2 - p^2)/Q^2$ . Making use of the definition of the electromagnetic current in Eq. (14), the elastic structure functions for the off-shell nucleon are then given by

at very low energies ( $E \approx 0.2$  GeV) from MIT-Bates, and by Arnold *et al.* [34] at higher energies ( $E \approx 1$  GeV) from SLAC. More extensive data sets from SLAC were collected in the early 1990s by Lung [35] around the QE peak for a range of scattering angles  $\theta \approx 15^\circ - 90^\circ$  at energies  $E \approx 1.5 - 5.5$  GeV, and by Rock *et al.* [36] at forward angles ( $\theta = 10^\circ$ ) at higher energies,  $E \approx 10 - 20$  GeV. The latter offered access to the highest available  $Q^2$  values, reaching  $Q^2 = 10$  GeV<sup>2</sup>. SLAC data with  $Q^2$  between 1 and 7 GeV<sup>2</sup> were also collected in the NE18 experiment [37] at  $x \approx 1$ . High precision data from Jefferson Lab were measured by Arrington *et al.* [38] at  $\theta \approx 15^\circ - 50^\circ$  for energies between  $E \approx 2$  and 5 GeV, and most recently by Fomin *et al.* [39] in the vicinity of  $x = 1$  using the 6-GeV CEBAF electron beam at angles between  $\theta \approx 18^\circ$  and  $50^\circ$ .

The complete QE data set amounts to over 2000 data points covering a range of  $Q^2$  between 0.1 and 10 GeV<sup>2</sup> for energies between  $E \approx 0.2$  and 20 GeV, from  $x \lesssim 1$  to  $x \approx 2$ . In particular, the angular dependence of the cross sections allows the effects of the  $F_1^d$  and  $F_2^d$  structure function contributions to be studied independently. Fitting these constitutes a significant test of any model of the deuteron.

#### B. Phenomenological analysis

Typical deuteron QE spectra are illustrated in Figs. 2 and 3, where the cross sections are calculated in the WBA model and compared with SLAC data from Lung [35]. The calculations were performed using several different deuteron wave functions, based on the Paris [30], WJC-1 [28], and CD-Bonn [29] nucleon-nucleon potentials, and elastic nucleon

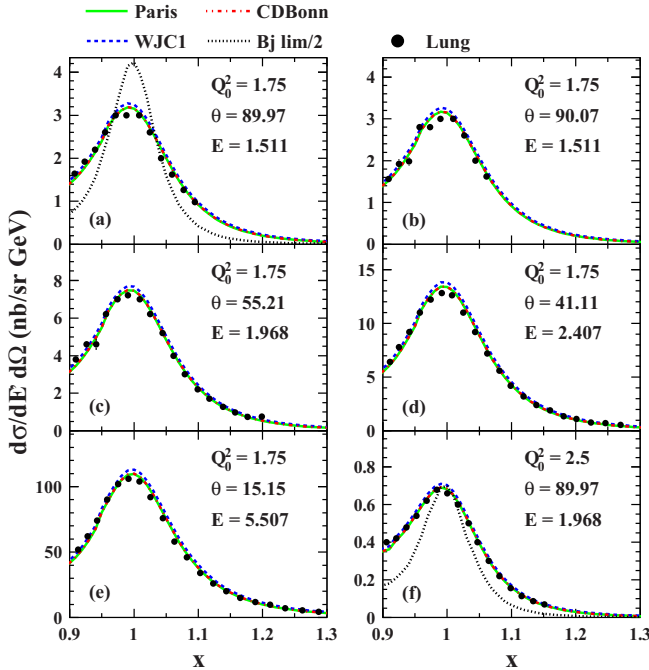


FIG. 2. (Color online) Inclusive electron-deuteron scattering cross section  $d\sigma/dE'd\Omega$  (in units of nb/sr GeV) in the QE region. The SLAC data from Lung [35] (solid circles) are compared with the WBA model predictions using the Paris [30] (green solid curves), WJC-1 [28] (blue dashed curves), and CD-Bonn (red dot-dashed curves) [29] deuteron wave functions. The results using the smearing functions computed in the large- $Q^2$  limit (black dotted curves) are also shown (scaled by a factor of 1/2 for clarity). In this and subsequent figures, the energy  $E$  (in GeV) and scattering angle  $\theta$  (in degrees) are indicated on each panel;  $Q_0^2$  (in  $\text{GeV}^2$ ) is the value of the four-momentum transfer squared at  $x = 1$ , which ranges here from  $Q_0^2 \approx 1.75$  to  $2.5 \text{ GeV}^2$ .

form factors from the parametrizations of Arrington *et al.* [40] for the proton and Bosted [41] for the neutron. Overall the agreement between the calculated cross sections and the data is excellent. This conclusion is independent of the choice of input nucleon elastic form factors, with the results using the parametrization of Kelly [42] differing from those in Figs. 2 and 3 by  $\lesssim 2\%$  for all kinematics. Furthermore, in the  $x$  range spanned by these data,  $x \lesssim 1.2$ , the QE cross sections display very mild dependence on the deuteron wave function.

In particular, the correct shape and magnitude of the QE peak is well reproduced with the  $y$ - and  $\gamma$ -dependent smearing functions of Eq. (12). In contrast, using the smearing functions computed in the high- $Q^2$  ( $\gamma \rightarrow 1$ ) limit, as appropriate for deep-inelastic scattering applications, the peak in the QE cross section would be a factor of  $\approx 2$  too large in the  $Q^2$  range ( $\sim 2 \text{ GeV}^2$ ) covered by the data in Figs. 2 and 3. At significantly higher  $Q^2$  ( $\gtrsim 10 \text{ GeV}^2$ ) the differences between the full, finite- $Q^2$  results and the high- $Q^2$  approximation are reduced, but at values relevant to most of the existing data the correct  $Q^2$  dependence of the smearing functions is vital to take into account.

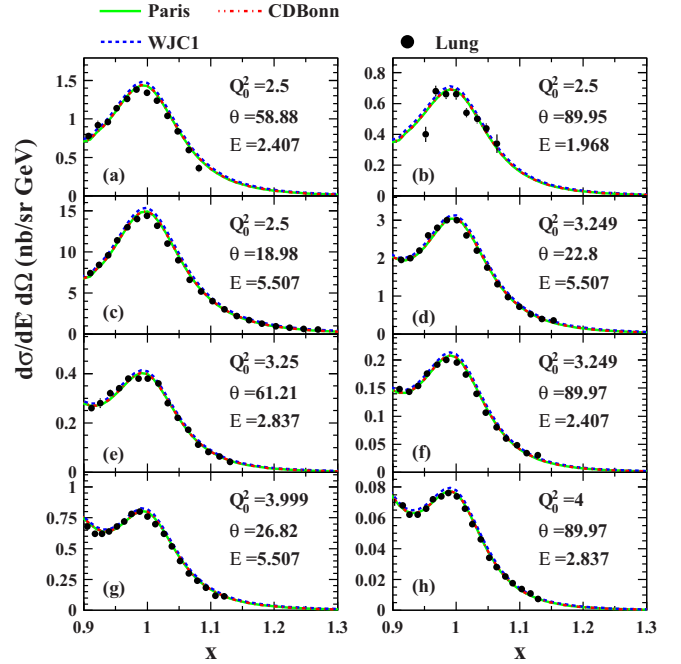


FIG. 3. (Color online) As in Fig. 2 but for  $Q_0^2$  between 2.5 and  $4 \text{ GeV}^2$ .

The excellent agreement between the WBA model predictions and the data holds over an even greater region of  $Q^2$  than that shown in Figs. 2 and 3. Data from the SLAC NE18 [37] and Jefferson Lab E89-008 [38] experiments spanning the range  $Q^2 \approx 1\text{--}7 \text{ GeV}^2$  are also well reproduced by the WBA model, as Fig. 4 demonstrates. The larger  $Q^2$  coverage allows one to study the relative importance of inelastic contributions at  $x \sim 1$  compared with the QE contribution. While the cross sections are dominated by QE scattering at  $x \gtrsim 1$  for  $Q^2 \lesssim 3 \text{ GeV}^2$ , at higher  $Q^2$  and lower  $x$  [or larger  $W^2 = (p + q)^2$ ] the role of inelastic scattering from the nucleon becomes increasingly more prominent. To reproduce the full strength of the inclusive cross section data in this region one must therefore add the inelastic contribution to the QE contribution.

The inelastic cross sections can be computed within the WBA framework using the same smearing functions as those in Eq. (12), convoluted with appropriate inelastic free nucleon structure functions as in Eqs. (11). A number of studies of inelastic deuteron structure functions have previously been performed in the literature [14–17,27], and the smearing functions have been used to extract information on the free neutron structure function [23,43,44] and on parton distribution functions at large  $x$  in global QCD analyses [45–49]. Rather than repeat these analyses, for the purposes of the present study it is sufficient to simply employ the inelastic contribution in the  $F_1^d$  and  $F_2^d$  structure functions as parametrized in the phenomenological analysis of Christy and Bosted [50]. As evident from Fig. 4, the inelastic contributions become relevant at  $x \lesssim 1$  for  $Q^2 \gtrsim 4 \text{ GeV}^2$ , although for  $x \gtrsim 1$  or  $Q^2 \lesssim 2\text{--}3 \text{ GeV}^2$  the cross sections are still dominated by the QE component alone.

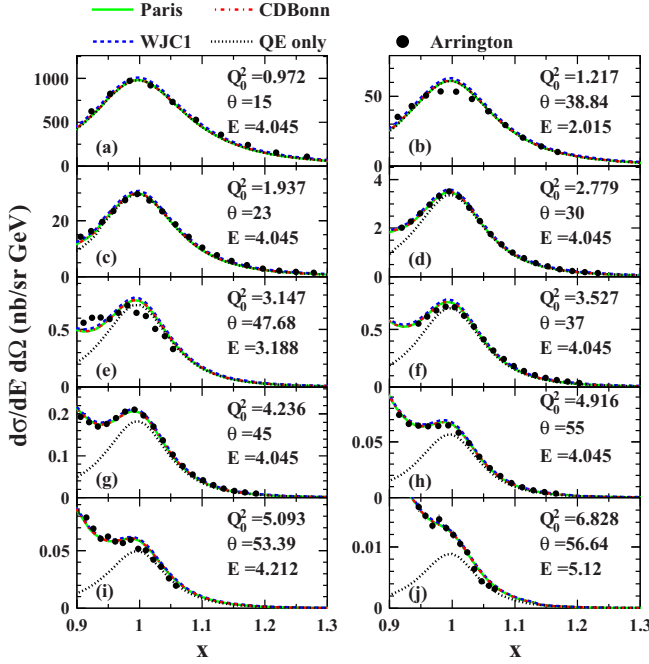


FIG. 4. (Color online) Inclusive electron-deuteron QE scattering cross sections in the WBA model using the Paris [30] (green solid curves), WJC-1 [28] (blue dashed curves), and CD-Bonn [29] (red dot-dashed curves) [29] deuteron wave functions, compared with Arrington *et al.* data from (b, e, i, j) the SLAC NE18 experiment [37] and (a, c, d, f-h) the Jefferson Lab E89-008 experiment [38] at  $E = 4.045$  GeV, for which  $Q_0^2$  ranges between  $\approx 1$  and  $7$  GeV $^2$ . The contributions from the QE scattering alone (black dotted curves) are shown for comparison.

Yet higher  $Q^2$  values were reached in the earlier SLAC experiment [36] at small scattering angles ( $\theta = 10^\circ$ ), where energies between  $E \approx 10$  and  $20$  GeV allowed for  $Q^2$  values up to  $10$  GeV $^2$ . As Fig. 5 illustrates, once again the agreement is generally good at  $x > 1$ , although curiously there appears a mismatch in the position of the QE peak at  $x \sim 1$ , which is most evident at the lower  $Q^2$  values,  $Q^2 \approx 2-4$  GeV $^2$ . This discrepancy appears difficult to reconcile with the otherwise excellent agreement between the WBA model and data from other experiments at SLAC [35,37] and Jefferson Lab [38] at similar kinematics, as evident in Figs. 2-4 (see also Fig. 11 below). Note also that for the highest- $Q^2$  panel the theoretical curves extend only to  $x \approx 1.1$ , corresponding to the maximum  $Q^2$  values up to which the elastic form factors parametrizations are given [40-42].

At very high values of  $x$  ( $x \gg 1$ ), QE scattering from the deuteron probes the tails of the smearing functions  $f_{ij}(y)$  at  $y \gg 1$ . As evident from Eq. (9), large- $y$  kinematics is sensitive to large nucleon momenta  $\mathbf{p}$  or, equivalently, to the short-range part of the  $NN$  interaction (see Fig. 1). Unlike the long-distance component of the  $NN$  potential, which is well constrained by  $pp$  and  $pn$  scattering data, the short-distance (or large-momentum) part of the deuteron wave function has relatively large uncertainties. This translates into a larger spread in the theoretical calculation of the deuteron structure functions when various models for the wave function are used.

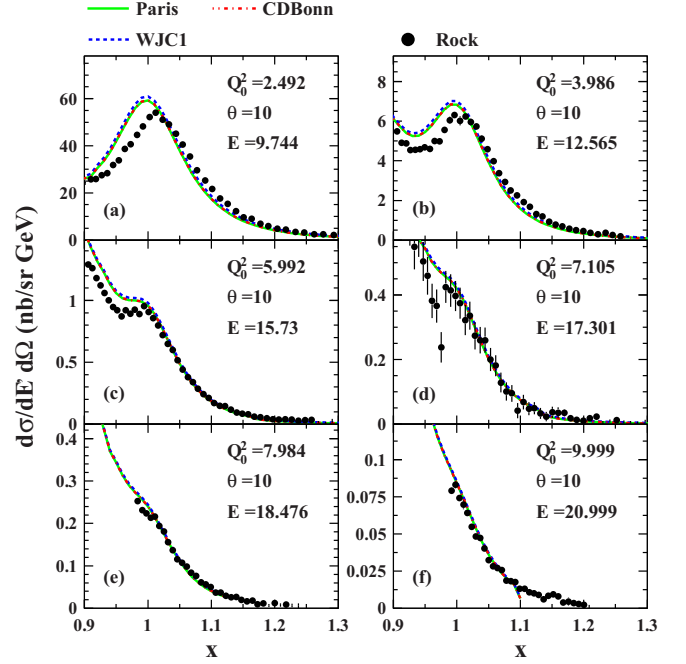


FIG. 5. (Color online) As in Fig. 4 but compared with the forward angle SLAC data from Rock *et al.* [36] at  $\theta = 10^\circ$ , with  $Q_0^2$  between  $\approx 2.5$  and  $10$  GeV $^2$ .

This is indeed observed in Fig. 6, where data from SLAC [32] at near-forward scattering angles are compared with the QE cross sections computed using the Paris [30], WJC-1 [28], and CD-Bonn [29] wave functions. As evident from the light-cone

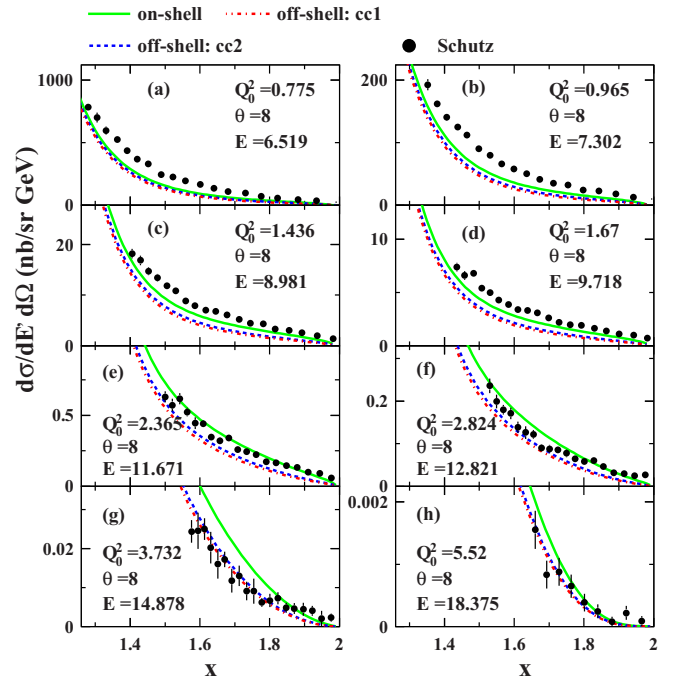


FIG. 6. (Color online) As in Fig. 4 but for the SLAC data from Schutz *et al.* [32] at small scattering angles, for  $Q_0^2$  ranging from  $\approx 0.8$  to  $\approx 5.5$  GeV $^2$ .

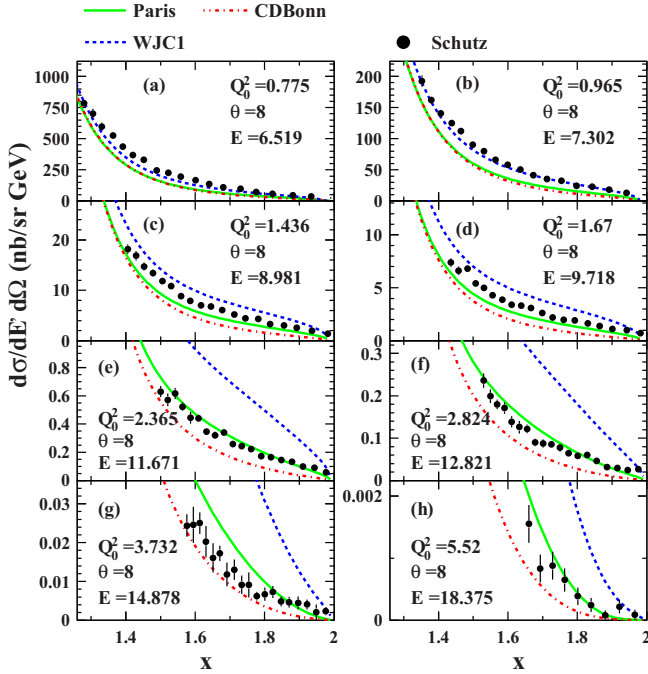


FIG. 7. (Color online) Comparison of the WBA model predictions for the QE electron-deuteron scattering at large  $x$ , using on-shell nucleon form factors (green solid curves) and the two off-shell model extrapolations in Eqs. (19) (off-shell cc2, blue dashed curves) and (20) (off-shell cc1, red dot-dashed curves). The Paris [30] deuteron wave function is used in all cases, and the data are as in Fig. 6.

momentum distributions in Fig. 1, generally the CD-Bonn model gives rise to the softest distribution, while the WJC-1 potential has the hardest distribution, with the Paris wave function intermediate between these. At the lower  $Q^2$  values the data tend to prefer the harder distributions, while softer wave functions are favored at increasingly larger  $Q^2$ .

In the same high- $x$  region where the uncertainties in the short-range structure of the deuteron yield greater model dependence of the QE cross sections, the effects of the possible off-shell dependence of the nucleon elastic cross section are also expected to become more important. In Fig. 7 the WBA predictions for the cross sections using on-shell nucleon form factors as in Eqs. (18) are compared with calculations using the off-shell structure functions from Eqs. (19) and (20) in the generalized convolution of Eqs. (8). For a meaningful comparison, the Paris deuteron wave function is used for all cases. The off-shell results with either the cc1 or cc2 models generally soften the distributions relative to the on-shell cross sections at high  $x$ , with the effects more pronounced with increasing  $Q^2$ . The off-shell corrections with the cc1 model are slightly larger in magnitude than those with the cc2 model, although the difference between these is significantly smaller than the difference between the on-shell and off-shell results.

Compared with the high- $x$  Schutz *et al.* data from SLAC [32], at the lower  $Q^2$  values ( $Q^2 \approx 1-2 \text{ GeV}^2$ ) the off-shell corrections with the Paris wave function make the agreement slightly worse, confirming the findings in Fig. 6 that these data prefer harder deuteron wave functions. In this region the WJC-1 wave function with minimal off-shell corrections

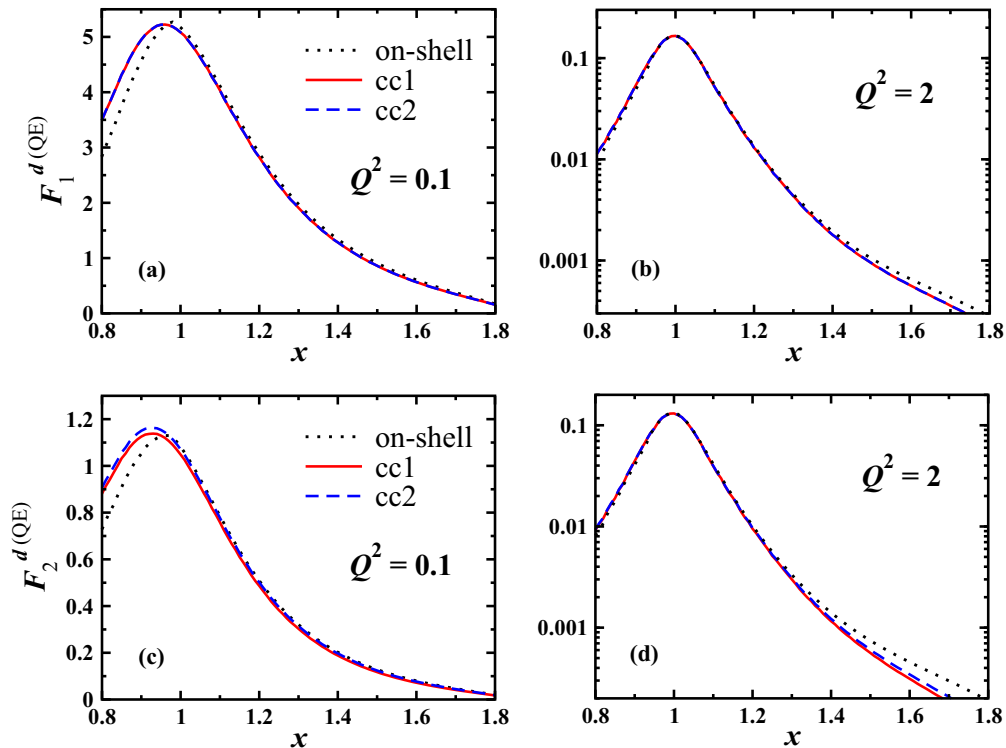


FIG. 8. (Color online) QE contributions to the deuteron (a, b)  $F_1^d$  and (c, d)  $F_2^d$  structure functions at  $Q^2 = 0.1 \text{ GeV}^2$  and  $Q^2 = 2 \text{ GeV}^2$ . The on-shell approximation (black dotted curves) is compared with the off-shell calculation using the cc1 (red solid curves) and cc2 (blue dashed curves) prescriptions, with the Paris wave function used in all cases.



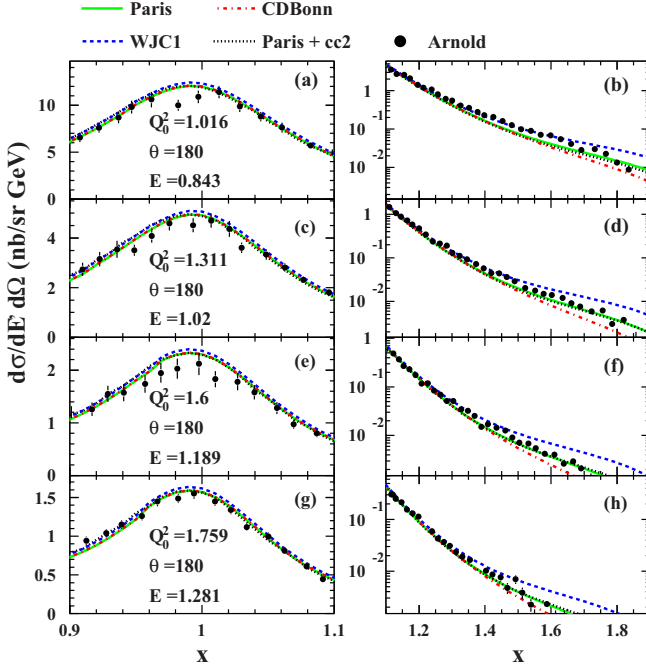


FIG. 9. (Color online) Deuteron wave function and nucleon off-shell model dependence of the QE cross sections at backward angles for  $Q_0^2$  between  $\approx 1$  and  $2 \text{ GeV}^2$ . The on-shell results for the Paris (green solid curves), WJC-1 (blue dashed curves), and CD-Bonn (red dot-dashed curves) wave functions, and the cc2 off-shell model with the Paris wave function (black dot-dashed curves), are compared with the SLAC data from Arnold *et al.* [34]. The left-hand panels illustrate the data in the vicinity of  $x = 1$  on a linear scale, while the right-hand panels show the tails of the cross sections at larger  $x$  on a logarithmic scale.

provides the best description of the data. At higher  $Q^2$  values ( $Q^2 \approx 2\text{--}6 \text{ GeV}^2$ ), using the hardest, WJC-1 wave function would require significantly larger off-shell corrections to reduce the excess of the calculated cross section relative to the data. The best agreement with data here is obtained with the softer Paris wave function, together with the off-shell nucleon form factors in Fig. 7. However, the softest wave function, with the CD-Bonn potential, would underestimate the cross sections with the addition of the off-shell nucleon corrections over all the kinematics in Fig. 7.

The behavior of the cross sections in Fig. 7 can be understood from the effects of the off-shell corrections on the  $F_1$  and  $F_2$  structure functions in Eqs. (19) and (20). In Fig. 8 the QE contributions to the deuteron  $F_1^d$  and  $F_2^d$  structure functions with and without off-shell corrections are shown at  $Q^2 = 0.1$  and  $2 \text{ GeV}^2$  for the cc1 and cc2 models. Overall, the off-shell effects on the structure functions are relatively small and weakly dependent on the choice of off-shell prescription. At low  $Q^2$  ( $Q^2 = 0.1 \text{ GeV}^2$ ) the off-shell corrections are noticeable only at  $x \lesssim 1$ , where they increase the magnitude of the  $F_1^d$  and  $F_2^d$  structure functions by  $\sim 10\text{--}20\%$ . At higher  $Q^2$  values ( $Q^2 = 2 \text{ GeV}^2$ ), the off-shell effects reduce the magnitude of the structure functions at high  $x$  ( $x \gtrsim 1.4$ ), with a slightly larger correction appearing for  $F_2^d$  than for  $F_1^d$ ,

particularly for the cc1 model. This explains the suppression observed in the QE cross sections at high  $x$  and  $Q^2$  in Fig. 7, where the forward angle data are dominated by the  $F_2^d$  contribution [see Eq. (4)].

At extreme backward angles ( $\theta = 180^\circ$ ) the dominance of magnetic scattering means that the cross section is given entirely by the  $F_1^d$  structure function. Backward angle data from SLAC at  $Q^2 \sim 1\text{--}2 \text{ GeV}^2$  [34] are compared in Fig. 9 with WBA calculations over the range  $0.9 \lesssim x \lesssim 1.8$ , including both deuteron wave function and nucleon off-shell effects. The overall agreement is very good, with the model dependence in the region of the QE peak,  $0.9 \lesssim x \lesssim 1.1$ , essentially negligible. (The results using the cc1 off-shell prescription are almost indistinguishable from those of the cc2 model shown in Fig. 9.) At larger  $x$  values the wave function dependence becomes more prominent, with the data at  $x \lesssim 1.5$  better described using the WJC-1 model, while the Paris wave function gives better agreement at higher  $x$ . The softer CD-Bonn wave function tends to underestimate the data at the highest  $x$ , as observed for the forward scattering angle data in Fig. 6. The off-shell corrections give a slight enhancement of the cross section at  $x \lesssim 1$ , which is consistent with the behavior of  $F_1^d$  around the QE peak in Fig. 8, but is otherwise negligible at these kinematics.

While a small, few percent enhancement of the backward angle QE cross section at  $x \lesssim 1$  due to off-shell effects is expected from Fig. 8 at  $Q^2 \approx 1\text{--}2 \text{ GeV}^2$ , since the off-shell corrections in Eqs. (19) and (20) scale with  $(M^2 - p^2)/Q^2$ , the effects should be somewhat larger at lower  $Q^2$  values. This is indeed observed in Fig. 10, where low-energy data from MIT-Bates [33] at  $Q^2 \sim 0.1\text{--}0.2 \text{ GeV}^2$  indicate an

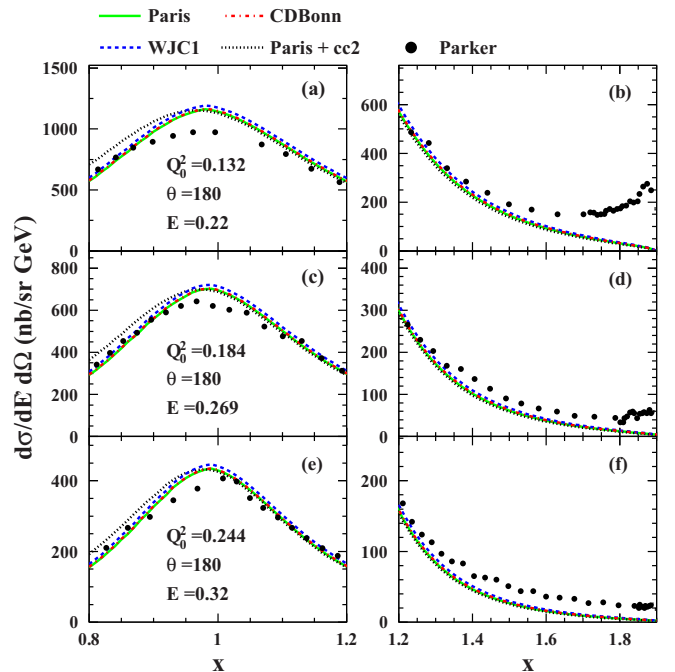


FIG. 10. (Color online) As in Fig. 9, but for the lower- $Q^2$  backward angle MIT-Bates data from Parker *et al.* [33], for  $Q_0^2 \sim 0.1\text{--}0.2 \text{ GeV}^2$ .

$\approx 10\text{--}20\%$  enhancement at  $x \approx 0.9$  compared with the on-shell cross section. The cross sections with the cc2 off-shell model are displayed in Fig. 10 (the results with the cc1 model are again almost indistinguishable), and the behavior follows directly from the off-shell correction to  $F_1^d$  at low  $Q^2$  illustrated in Fig. 8.

At the low- $Q^2$  values of the backward angle MIT-Bates data from Parker *et al.* in Fig. 10, the dependence on the deuteron wave function is very weak, even at large values of  $x$ . All models appear to slightly overestimate the data in the  $x \sim 1$  region, possibly suggesting a role for meson exchange currents at these kinematics. Interactions between the virtual photon and a meson exchanged between the two nucleons in the deuteron are known to affect the  $F_1$  structure function more so than the  $F_2$  structure function in QE electron-deuteron scattering [51]. The agreement between the calculations and data at  $x \gtrsim 1$  is very good, although at larger  $x$  ( $x \gtrsim 1.3$ ) the calculation using the Paris wave function somewhat underestimates the data. As observed for the forward angle data in Fig. 6, here the harder momentum distribution associated with the WJC-1 deuteron wave function would produce better agreement. As for the higher  $Q^2$  backward angle data in Fig. 9, the off-shell corrections play a minor role in this region. For even higher  $x$ , the data exhibit a significant rise as  $x \rightarrow 2$ , especially at lower  $Q^2$ , which is likely due to the elastic electron-deuteron scattering contribution, which drops rapidly with increasing  $Q^2$ .

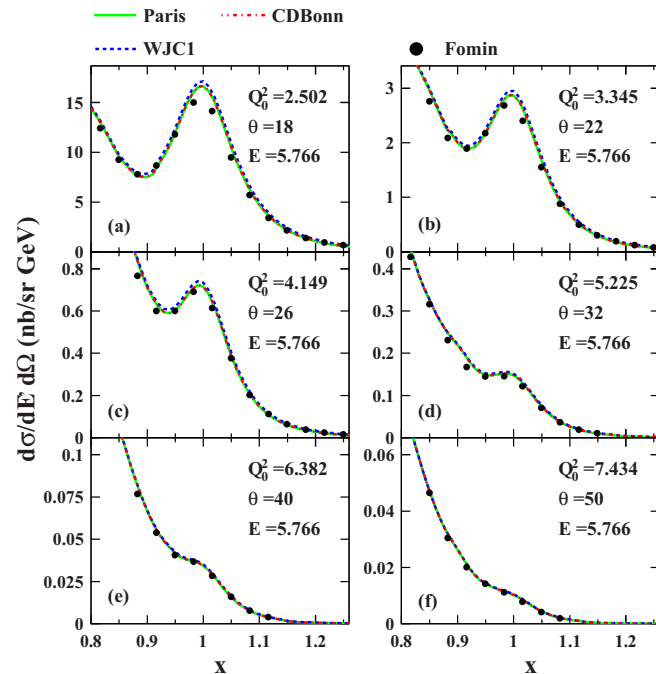


FIG. 11. (Color online) Inclusive electron-deuteron QE scattering cross sections in the WBA model using the Paris [30] (green solid curves), WJC-1 [28] (blue dashed curves), and CD-Bonn (red dot-dashed curves) [29] deuteron wave functions, compared with data from the E02-019 experiment in Hall C at Jefferson Lab. The incident energy is  $E = 5.766$  GeV, with the scattering angles ranging from  $\theta = 18^\circ$  to  $50^\circ$ , and  $Q_0^2$  values from 2.5 to 7.4  $\text{GeV}^2$ .

Finally, the very latest and precise data on QE electron-deuteron scattering from the Hall C experiment E02-019 at Jefferson Lab [39] are shown in Fig. 11, spanning a range of  $Q^2$  between  $\approx 2$  and 8  $\text{GeV}^2$  and scattering angles between  $\theta \approx 18^\circ$  and  $50^\circ$ . The agreement between the WBA model and the data is clearly excellent over the complete  $x$  range ( $x \lesssim 1.25$ ) covered, with very mild dependence on the deuteron wave function. The effects of nucleon off-shell corrections are also negligible at these kinematics. This close correspondence between the theory and experiment provides further indication of the general success of the WBA approach to describing inclusive electron-deuteron scattering.

#### IV. CONCLUSIONS

We performed a comprehensive analysis of QE electron-deuteron scattering data within the framework of the weak-binding approximation. Using the same smearing functions for the bound nucleons in the deuteron as those previously derived for deep-inelastic scattering at finite  $Q^2$ , we explored the limits of applicability of the impulse approximation in the WBA. Overall, we find excellent agreement between the model calculations and the world's available data over a large range of kinematics, covering  $Q^2$  values between  $\sim 0.1$  and 10  $\text{GeV}^2$ , and  $x$  values from below the QE peak to  $x \approx 2$ . It is vital, however, that the correct kinematical  $Q^2$  dependence in the smearing function is taken into account in order to describe the cross section data, in contrast to the high- $Q^2$  approximation that can usually be assumed for deep-inelastic scattering.

The results are relatively independent of the details of the deuteron wave function, except at very high values of  $x$  ( $x \gtrsim 1.3$ ) and  $Q^2 \gtrsim 1$   $\text{GeV}^2$ , where there is greater sensitivity to the high-momentum tails of the nucleon momentum distributions in the deuteron. For  $Q^2 \sim 1$   $\text{GeV}^2$  the wave function based on the WJC-1 nucleon-nucleon potential [28], which has the hardest momentum distribution, provides the best agreement with the QE data, while for  $Q^2 \gtrsim 2$   $\text{GeV}^2$  the Paris wave function [30] gives the best fit. The CD-Bonn potential [29], with the softest momentum distribution, tends to underestimate the data at the highest  $x$  and  $Q^2$  values. This suggests that QE data at these kinematics could be used to constrain the short-distance part of the  $NN$  interaction, as reflected in the high-momentum behavior of the smearing functions.

At high  $x$  and low  $Q^2$  corrections from nucleon off-shell effects are also expected to play a role. We considered two models for extrapolating the nucleon electromagnetic current off-shell, corresponding to the cc1 and cc2 prescriptions commonly used in the literature [31]. Uncertainties in the off-shell corrections to structure functions of nucleons in the deuteron is one of the main impediments to the unambiguous extraction of the free neutron structure and the determination of the  $u$  and  $d$  parton distribution functions at large  $x$  [12,13,44–48]. Studies of QE scattering can therefore provide additional information on the off-shell corrections which could better constrain the parton distribution function analyses. In practice, we find relatively small off-shell corrections for most kinematics, with the exception of very low  $Q^2$  ( $Q^2 \sim 0.1\text{--}0.2$   $\text{GeV}^2$ ) at  $x \lesssim 1$ , where the off-shell effects increase the on-shell cross sections, and at very high  $x$  ( $x \gtrsim 1.4$ ) for  $Q^2 \sim 1$   $\text{GeV}^2$ , where the

cross sections are slightly reduced by the off-shell effects. The dependence on the off-shell prescription (cc1 or cc2) appears insignificant at the kinematics where data currently exist.

In certain kinematic regions there are discrepancies between the calculations and some of the data sets, such as at very low  $Q^2$  values around the QE peak [33], where all calculations slightly overestimate the data. This may indicate a problem with the data, or perhaps the need for additional corrections not taken into account in this analysis. Since the data in question [33] are at extreme backward angles, where  $F_1^d$  dominates, this suggests that meson exchange currents may play a role, as these are known to be more important for the transverse response functions than for the longitudinal [51].

In general, however, the WBA model provides a remarkably good description of the QE data in all but the most extreme kinematics ( $x \gg 1$  and  $Q^2 \rightarrow 0$ ), which gives additional confidence in the use of the finite- $Q^2$  smearing functions to compute nuclear effects in other processes, such as inclusive deep-inelastic scattering [46–48]. In particular, the availability of QE data at both forward and backward scattering angles allows the effects on the  $F_1^d$  and  $F_2^d$  structure function contributions to be studied independently, and over a substantial range of  $x$  and  $Q^2$ . This poses a serious test of the model of the deuteron and provides clearer indications of the limits of applicability of the WBA approach. Recently, a phenomenological analysis of QE contributions to the Lamb shift in muonic deuterium was performed [52] including Fermi smearing and final state interaction effects. Parametrizing the

latter by simple functional forms, the impulse approximation was also found to give a good description of the data up to  $Q^2 = 3 \text{ GeV}^2$ , similar to the findings in our analysis.

As far as the implications for future work, additional data at high  $x$  ( $x \gtrsim 1.5$ ) and high  $Q^2$ , at forward and backward angles, would be very helpful in constraining the model dependence of the deuteron wave function, and possibly teasing out the off-shell dependence of the nucleon structure functions. On the theoretical front, inclusion of the QE deuteron data in studies of  $NN$  scattering could allow for a more reliable determination of the large-momentum components of the deuteron wave function. For precision fits to the QE data, it will be necessary to explore quantitatively in addition meson exchange currents, rescattering (or final state interaction) effects, and the relativistic motion of nucleons in the deuteron. The present study should provide an important baseline for these additional contributions.

## ACKNOWLEDGMENTS

We thank J. Arrington, D. Day, S. Kulagin, A. Lung, and J. W. Van Orden for helpful discussions and communications. This work was supported by the U.S. DOE Contract No. DE-AC05-06OR23177, under which Jefferson Science Associates, LLC, operates Jefferson Lab. N.D. acknowledges support from DOD's ASSURE program and NSF Grant No. 1062320 for an REU internship at ODU/Jefferson Lab.

- 
- [1] G. B. West, *Phys. Lett. B* **37**, 509 (1971).  
 [2] R. L. Jaffe, in *Relativistic Dynamics and Quark-Nuclear Physics*, edited by M. B. Johnson and A. Pickleseimer (Wiley, New York, 1985).  
 [3] R. L. Jaffe and A. Manohar, *Nucl. Phys. B* **321**, 343 (1989).  
 [4] W. Cosyn, W. Melnitchouk, and M. Sargsian, *Phys. Rev. C* **89**, 014612 (2014).  
 [5] W. Cosyn and M. Sargsian, *Phys. Rev. C* **84**, 014601 (2011).  
 [6] C. Ciofi degli Atti, L. P. Kaptari, and D. Treleani, *Phys. Rev. C* **63**, 044601 (2001).  
 [7] C. Ciofi degli Atti, L. P. Kaptari, and B. Z. Kopeliovich, *Eur. Phys. J. A* **19**, 145 (2004).  
 [8] V. Palli, C. Ciofi degli Atti, L. P. Kaptari, C. B. Mezzetti, and M. Alvioli, *Phys. Rev. C* **80**, 054610 (2009).  
 [9] L. P. Kaptari and A. Yu. Umnikov, *Phys. Lett. B* **272**, 359 (1991).  
 [10] W. Melnitchouk and A. W. Thomas, *Phys. Rev. D* **47**, 3783 (1993).  
 [11] F. Gross and S. Liuti, *Phys. Rev. C* **45**, 1374 (1992).  
 [12] W. Melnitchouk, A. W. Schreiber, and A. W. Thomas, *Phys. Rev. D* **49**, 1183 (1994).  
 [13] W. Melnitchouk, A. W. Schreiber, and A. W. Thomas, *Phys. Lett. B* **335**, 11 (1994).  
 [14] S. A. Kulagin, G. Piller, and W. Weise, *Phys. Rev. C* **50**, 1154 (1994).  
 [15] S. I. Alekhin, S. A. Kulagin, and S. Liuti, *Phys. Rev. D* **69**, 114009 (2004).  
 [16] S. A. Kulagin and R. Petti, *Nucl. Phys. A* **765**, 126 (2006).  
 [17] Y. Kahn, W. Melnitchouk, and S. A. Kulagin, *Phys. Rev. C* **79**, 035205 (2009).  
 [18] S. A. Kulagin, W. Melnitchouk, G. Piller, and W. Weise, *Phys. Rev. C* **52**, 932 (1995).  
 [19] S. A. Kulagin and W. Melnitchouk, *Phys. Rev. C* **78**, 065203 (2008).  
 [20] S. A. Kulagin and W. Melnitchouk, *Phys. Rev. C* **77**, 015210 (2008).  
 [21] J. J. Ethier and W. Melnitchouk, *Phys. Rev. C* **88**, 054001 (2013).  
 [22] S. P. Malace *et al.*, *Phys. Rev. C* **80**, 035207 (2009).  
 [23] S. P. Malace, Y. Kahn, W. Melnitchouk, and C. E. Keppel, *Phys. Rev. Lett.* **104**, 102001 (2010).  
 [24] W. Melnitchouk, R. Ent, and C. E. Keppel, *Phys. Rep.* **406**, 127 (2005).  
 [25] O. Benhar, D. Day, and I. Sick, [arXiv:nucl-ex/0603032](http://arxiv.org/abs/nucl-ex/0603032); <http://faculty.virginia.edu/qes-archive>.  
 [26] O. Benhar, D. Day, and I. Sick, *Rev. Mod. Phys.* **80**, 189 (2008).  
 [27] A. Accardi, J. W. Qiu, and J. P. Vary (unpublished).  
 [28] F. Gross and A. Stadler, *Phys. Rev. C* **78**, 014005 (2008).  
 [29] R. Machleidt, *Phys. Rev. C* **63**, 024001 (2001).  
 [30] M. Lacombe *et al.*, *Phys. Lett. B* **101**, 139 (1981).  
 [31] T. De Forest, *Nucl. Phys. A* **392**, 232 (1983).  
 [32] W. P. Schutz *et al.*, *Phys. Rev. Lett.* **38**, 259 (1977).  
 [33] B. Parker *et al.*, *Phys. Rev. C* **34**, 2354 (1986).  
 [34] R. G. Arnold *et al.*, *Phys. Rev. Lett.* **61**, 806 (1988).  
 [35] A. Lung, Ph.D. thesis, American University, UMI-AAT 9322579, 1992 (unpublished).  
 [36] S. Rock *et al.*, *Phys. Rev. D* **46**, 24 (1992).

- [37] J. Arrington *et al.*, *Phys. Rev. C* **53**, 2248 (1996).
- [38] J. Arrington *et al.*, *Phys. Rev. Lett.* **82**, 2056 (1999); *Phys. Rev. C* **64**, 014602 (2001).
- [39] N. Fomin, Ph.D. thesis, University of Virginia, 2007, [arXiv:0812.2144](https://arxiv.org/abs/0812.2144) [nucl-ex]; N. Fomin *et al.*, *Phys. Rev. Lett.* **105**, 212502 (2010).
- [40] J. Arrington, W. Melnitchouk, and J. A. Tjon, *Phys. Rev. C* **76**, 035205 (2007).
- [41] P. E. Bosted, *Phys. Rev. C* **51**, 409 (1995).
- [42] J. J. Kelly, *Phys. Rev. C* **70**, 068202 (2004).
- [43] O. Hen, A. Accardi, W. Melnitchouk, and E. Piasetzky, *Phys. Rev. D* **84**, 117501 (2011).
- [44] J. Arrington, J. G. Rubin, and W. Melnitchouk, *Phys. Rev. Lett.* **108**, 252001 (2012).
- [45] S. Alekhin, J. Blümlein, S. Klein, and S.-O. Moch, *Phys. Rev. D* **81**, 014032 (2010).
- [46] A. Accardi, M. E. Christy, C. E. Keppel, W. Melnitchouk, P. Monaghan, J. G. Morfin, and J. F. Owens, *Phys. Rev. D* **81**, 034016 (2010).
- [47] A. Accardi, W. Melnitchouk, J. F. Owens, M. E. Christy, C. E. Keppel, L. Zhu, and J. G. Morfin, *Phys. Rev. D* **84**, 014008 (2011).
- [48] J. F. Owens, A. Accardi, and W. Melnitchouk, *Phys. Rev. D* **87**, 094012 (2013).
- [49] P. Jimenez-Delgado, W. Melnitchouk, and J. F. Owens, *J. Phys. G: Nucl. Part. Phys.* **40**, 093102 (2013).
- [50] M. E. Christy and P. E. Bosted, *Phys. Rev. C* **81**, 055213 (2010).
- [51] J. W. Van Orden and T. W. Donnelly, *Ann. Phys.* **131**, 451 (1981).
- [52] C. E. Carlson, M. Gorchtein, and M. Vanderhaeghen, *Phys. Rev. A* **89**, 022504 (2014).